PAPER • **OPEN ACCESS**

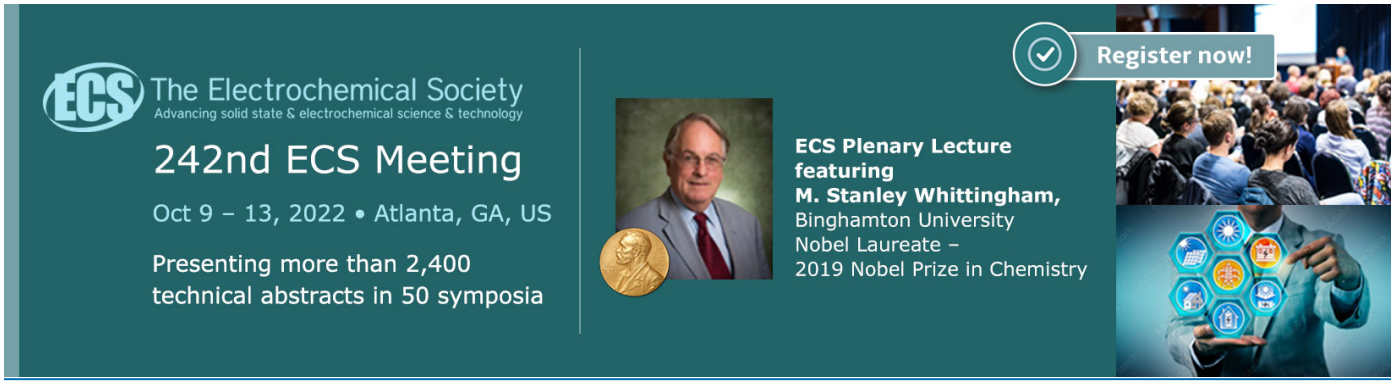
A flexible actuator curve model for aeroelastic simulations of wind turbines in atmospheric boundary layers

To cite this article: François Trigaux *et al* 2022 *J. Phys.: Conf. Ser.* **2265** 022050

View the article online for updates and enhancements.

You may also like

- Special issue on applied neurodynamics: from neural dynamics to neural engineering
Hillel J Chiel and Peter J Thomas
- Energy-band dynamics in a current-biased Josephson junction probed by incoherent Cooper-pair tunneling
Juha Leppäkangas and Erkki Thuneberg
- Summary of Papers
Serge Gauthier, Snezhana I Abarzhi and Katepalli R Sreenivasan



This content was downloaded from IP address 130.104.238.234 on 03/10/2022 at 15:20

A flexible actuator curve model for aeroelastic simulations of wind turbines in atmospheric boundary layers

François Trigaux, Philippe Chatelain and Grégoire Winckelmans
Institute of Mechanics, Materials and Civil Engineering (iMMC), Université catholique de Louvain (UCLouvain), 1348 Louvain-la-Neuve, Belgium

E-mail: `francois.trigaux@uclouvain.be`

Abstract. The current trend of wind turbine upscaling has led to the use of long and slender blades prone to large structural deformations. In the present study, the impact of the aeroelastic effects is assessed for the NREL-5MW wind turbine in a turbulent wind. To this end, an actuator curve method coupled to a one-dimensional finite-element structural solver is implemented in a fourth-order finite difference code that can perform large eddy simulation (LES) of realistic winds. The approach is computationally affordable compared to blade-resolved simulations and hence long time series can be computed. This, combined to the ability of the LES to capture the relevant scales of the unsteadiness wind, leads to a better estimation of the fluctuating loads and power of the turbine. The results are here shown for one and two wind turbines operating in a neutrally stable atmospheric boundary layer. It appears that the blade mostly deforms according to its first bending mode. The rotation of the blade in the sheared atmospheric flow is responsible for large amplitude deformations, but the turbulence also plays a role in causing deformations at higher frequencies with a smaller amplitude. The azimuthal distributions of loads and of power are significantly affected when the aeroelasticity is considered.

1. Introduction

In the recent years, there has been a clear trend in enlarging the wind turbines to increase their power extraction. These days, commercially available wind turbines can reach a rated power close to 12MW and their diameter exceeds 200 m. The rotor blades are more slender and manufactured using lightweight composite materials that add to the blade flexibility. Therefore, those new designs are more likely to exhibit significant aeroelastic effects in the form of unsteady deformations arising from the unsteady wind (mean wind shear and turbulent fluctuations) that modify the blades aerodynamics. Those effects can be beneficial if they provide passive load alleviation, but they can also deteriorate the turbine performance. A deeper understanding of the dynamic aeroelastic effects affecting a rotor in realistic turbulent wind conditions is hence required.

A wide spectrum of aeroelastic simulations exists in the literature. At one end, very detailed simulations resolve the flow around the blade geometry using the unsteady Reynolds Averaged Navier-Stokes (URANS) equations and use an accurate structural solver [1, 2, 3, 4, 5, 6, 7]. Those simulations require high computational capabilities. Moreover, the URANS equations are often also used for the wind field simulation itself; which does not capture the spectrum of


Content from this work may be used under the terms of the Creative Commons Attribution 3.0 licence. Any further distribution of this work must maintain attribution to the author(s) and the title of the work, journal citation and DOI.
Published under licence by IOP Publishing Ltd

the turbulent scales. Consequently, the fluctuation of the loads is not completely obtained.

On the other end of the spectrum, applications like HAWC2 and OpenFast use the blade element momentum (BEM) theory coupled to a one-dimensional structural solver. Although this decreases the computational cost, the absence of a detailed flow description hinders the simulation of realistic winds or multiple wind turbines.

In the middle of this spectrum lies the possibility to use an actuator disk, sector or line coupled to a one-dimensional structural solver in large eddy simulations (LES). This way, it becomes computationally affordable to simulate long time-series, also with multiple turbines. The use of LES allows to generate the full unsteadiness of the atmospheric wind and to accurately capture the relevant details of the unsteady wake behind the rotor. Some studies exist that use this method. Among them, Churchfield *et al.* [8] performed a study with rigid actuator lines but computed the forces using FAST, hence including structural deformation. Storey *et al.* [9] coupled an actuator disk method to FAST in their SnS code. More recently, Vitsas *et al.* [10] coupled an assumed-mode method with an actuator sector to simulate a two wind farm configurations. Sessarego *et al.* [11] coupled the HAWC2 structural solver to a three-dimensional viscous–inviscid interactive solver. Meng *et al.* or Spyropoulos *et al.* [12, 13] used a deformable actuator line in a URANS code to compare their result to a FAST or a BEM method. To the authors knowledge, a deformable actuator line method enabled in a LES code with a turbulent inflow has not yet been studied in depth. Such a development can provide more insights into the effects of the unsteady loads with a good accuracy.

In this study, a flexible actuator curve method is first presented. This method belongs to the category of the aforementioned actuator methods and has advantages similar to the actuator line, but it can also deform while maintaining a force distribution that minimizes the inaccuracies caused by the force mollification. It is combined with a one-dimensional finite-element structural solver to perform LES of wind turbines with flexible blades and in realistic atmospheric winds. Here, LES with rigid and elastic blades are carried on the NREL-5MW wind turbine model (from [14]) in various conditions, to compare and to highlight the importance of the structural deformations.

The next section describes the methodology developed for this work by presenting the actuator curve method, and its coupling with the structural solver. Then, some results are presented in Section 3. First, a verification of the method is carried by comparing the results obtained with a uniform velocity inflow to blade-resolved URANS simulations. Then, a comparison of a rotor with rigid or flexible blades is performed with a turbulent atmospheric boundary layer (ABL) as inflow. Finally, the aeroelastic effects on a turbine placed in the wake of a preceeding one, and both in the ABL, are also investigated.

2. Methodology

2.1. Flow solver

The LES of turbulent flows is considered. The incompressible Navier-Stokes equations supplemented by a subgrid scale model are solved using an in-house developed HPC and fourth-order finite differences code [15, 16]. A Smagorinsky subgrid scale model [17] further supplemented with a near-wall closure model (here for rough ground) is used. The mesh is a cartesian staggered grid and the time integration is performed using a second order Adams-Bashforth scheme. When the simulation of wind turbine(s) in an ABL is considered, two co-current simulations are used. The main one involves the wind turbine(s), while the auxiliary one is used to generate the inflow conditions that are directly transferred to the inlet of the main domain.

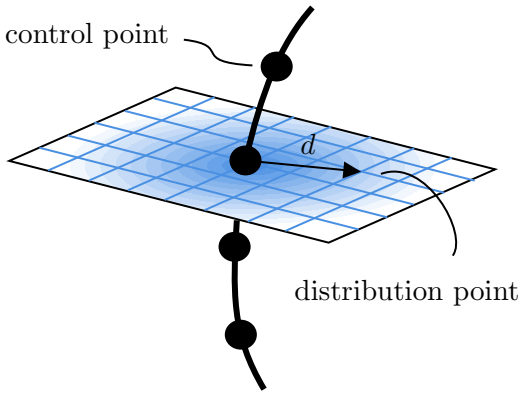


Figure 1: Schematic of the 2D distribution using a template plane perpendicular to the curve and with Gaussian weights.

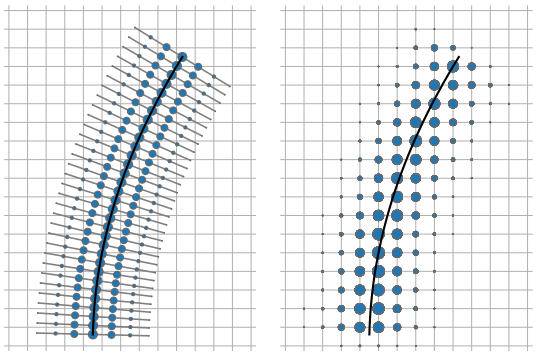


Figure 2: Illustration of the evolution of the weights after interpolation from the template planes to the flow grid points.

2.2. Actuator curve method

The actuator curve method is an extension of the actuator line method to curved blades. The original actuator line method introduced by *Sorensen and Shen* [18] allows for the simulation of wind turbines in three main steps. First, the flow velocity is interpolated from the flow grid to the control points that coincide with the turbine blades positions. Then, at those points, the aerodynamic forces are computed using experimental or computed airfoil data. Finally, the forces are distributed to the flow grid to be added as a forcing term to the LES equations. The actuator curve follows the same steps, but the control points are placed on a parametric curve and the orientation of the forces is modified accordingly [19]. Moreover, the distribution step is also modified from the original method.

Indeed, the forces distribution step can importantly affect the accuracy of the actuator line method. Typically, this step is performed as a convolution of the forces with a 3D Gaussian kernel that has a uniform width in each direction. Yet, it has been shown that the mollification in the spanwise direction leads to an overprediction of the aerodynamic forces, especially near the blade edges [20]. To avoid spanwise smearing, the actuator curve therefore distributes the forces in a plane perpendicular to the curve, as depicted on Figure 1. A 2D Gaussian kernel is used

$$\eta_{2D} = \frac{1}{\pi\sigma^2} \exp\left(-\frac{d^2}{\sigma^2}\right).$$

where d is the distance to the control point in the plane and σ the width of the Gaussian.

Performing a 2D distribution along a curve onto a cartesian mesh can be difficult [19]. To facilitate that process, a planar template containing so-called distribution points with their pre-computed Gaussian weights is attached to each control point. Those planes are translated and rotated so as to remain perpendicular to the curve at each control point. Linear interpolation is then used to transfer the content of those distribution points to the flow grid, as illustrated in Figure 2.

2.3. Structural solver

The structural analysis of the blades is performed using one-dimensional beam theories. Either the Euler-Bernoulli classical beam theory (EBBT) or the geometrically exact beam theory (GEBT) [21] are used. The latter is particularly suited to study the structural deformations of long wind turbines blades. It is able to capture large blade displacements and the material properties of each blade cross-section is represented using a full 6×6 matrix, allowing the

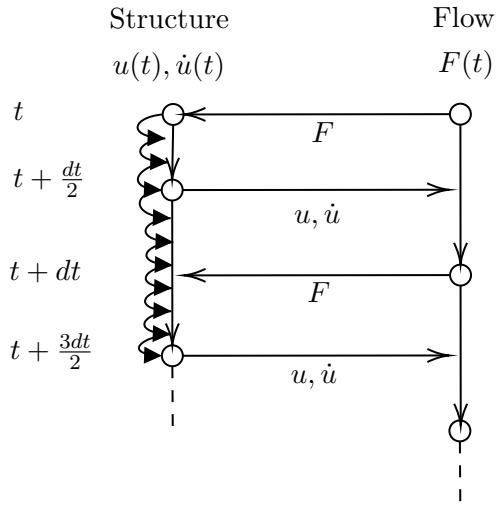


Figure 3: The coupling methodology. The flow solver sends the loads $F(t)$ to the structural solver which sends in return the displacements and velocities $u(t+dt/2)$ and $\dot{u}(t+dt/2)$. Those values are evaluated in a staggered way and sub-stepping is used at the structural solver level.

representation of composite materials and elastic coupling effects (such as bend-twist coupling). However, the NREL-5MW blade does not present such coupling and is not that long; it is hence unlikely to undergo significantly large displacements for typical load cases and the EBBT assumptions remain valid for this turbine.

A finite element model is used to solve the aforementioned beam models. The EBBT is represented using 3rd order beam elements [22]. A second order Newmark scheme is used for the transient analysis. The linear system that arises from the finite element discretization is solved using the PETSc library [23]. The GEBT simulation is carried using the eponymous open source GEBT code [24]. This solver uses linear finite elements to solve the mixed formulation of the GEBT equations and Wiener-Milenkovic parameters are used for the rotations. The original implementation of the equations does not include a damping term. Damping is required to maintain stability during aeroelastic simulations over long times. Consequently, a viscous damping term proportional to the element stiffness was here added to the equilibrium equations.

A model for the NREL-5MW blade was developed specifically for both solvers. It was then compared to the results of BeamDyn [25] for typical load cases. An overall good agreement was found with the GEBT code. The EBBT code also performs very well for moderate load cases that do not induce large displacements. Section 3 will compare the results obtained using both models under realistic aerodynamic loads.

2.4. Coupling

An explicit Improved Serial Staggered (ISS) scheme is used to couple the actuator curve method to the structural solver [26]. A schematic of this scheme is provided in Figure 3. The flow solver provides the aerodynamic loads $F(t)$ at time t to the structural solver which uses them as input for the dynamic analysis. This structural analysis is carried by substeps until $t + dt/2$ is reached. Then, the displacements $u(t + dt/2)$ and velocities $\dot{u}(t + dt/2)$ are transferred back to the actuator curve control points. The aerodynamic loads are thus evaluated at a different time level than the structural displacements.

Table 1: Main results for the NREL-5MW rotor with uniform inflow: power, thrust, flapwise and edgewise tip deflections.

	Power [MW]	Thrust [kN]	Flap. u_{tip} [m]	Edge. u_{tip} [m]
Present results (rigid)	5.95	767.93	-	-
Present results (EBBT)	5.66	737.54	5.03	-0.62
Present results (GEBT)	5.61	733.84	5.12	-0.65
Dose (rigid) [6]	5.51	761.7	-	-
Dose (flexible) [6]	5.49	771.3	5.55	-0.62

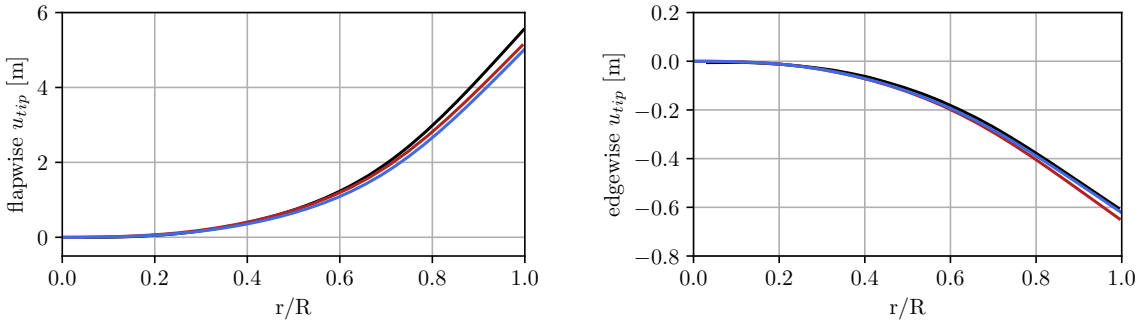


Figure 4: Blade deflection: Actuator curve with EBBT model (blue), GEBT model (red) compared to the reference results of *Dose* (black).

3. Results

3.1. The NREL-5MW rotor in uniform flow

First, verification results obtained for the NREL-5MW rotor submitted to a uniform inflow are presented. The inflow velocity is 11.4 m/s and the rotor rotation speed is fixed to 12.1 rpm. The computational setup is a domain of size $8D$ in the streamwise direction, and $6D$ in the two transverse directions, where $D = 126$ m is the rotor diameter. Periodic conditions are enforced on the lateral boundaries. The mesh consists of a uniform cartesian grid with 64 grid points per rotor diameter. The time-step is set to $\Delta t = 0.01$ s and the simulation is run for a total of 120 s. The actuator curve consists of 32 control points per blade, whereas the structural solver has 24 elements.

Here, the results are compared with those of *Dose et al.* [6] who performed blade-resolved simulation using URANS equations combined with a in-house implementation of the GEBT for the structural part.

Table 1 contains the outputs of the simulations for three cases: a rigid rotor with no blade deformation, and flexible rotors with the structural displacement computed either with the EBBT or the GEBT models. In the rigid case, the actuator curve method overestimates the power by $\simeq 7.5\%$ whereas the thrust is predicted accordingly to the reference results. This is mainly due to an overestimation of the tangential forces near the blade tip. Interestingly, introducing flexibility affects the power and thrust by $\simeq 4\%$ when the actuator curve method is used, whereas the reference results do not show any major difference. The tip displacements obtained with the flexible actuator curve method agree well with the reference. For both cases, the flapwise tip deflection is a little under-predicted; contrary to the edgewise deflection.

Figure 4 shows the blade deflections, also compared to the results of *Dose*. The deflections of both cases correspond well, with some difference near the end of the blade, due to the difference

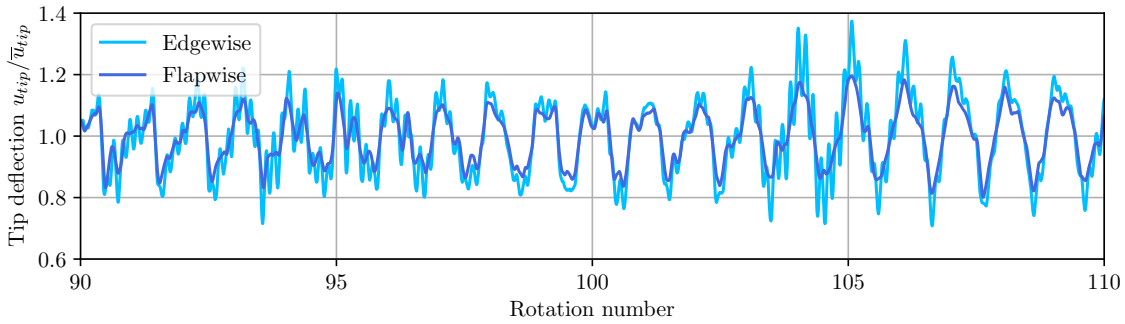


Figure 5: Instantaneous edgewise and flapwise blade tip deflections, each normalized by its mean deflection.

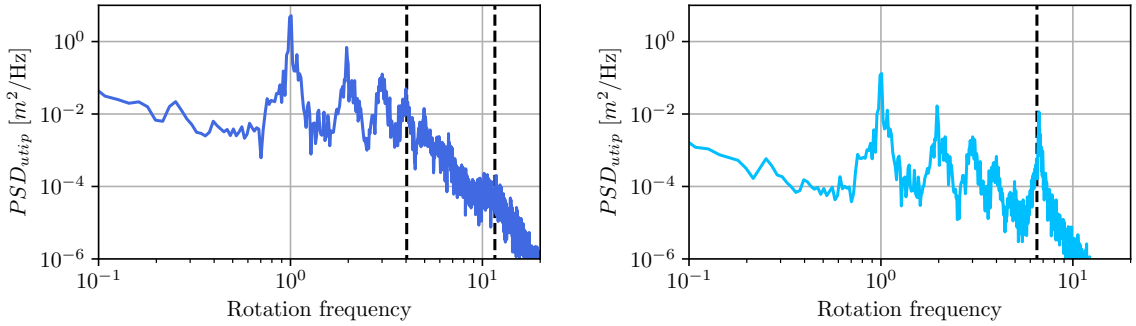


Figure 6: Power spectral density of the blade tip deflection for the flapwise (right) and edgewise (left) directions. The vertical dashed lines indicates the blade eigenfrequencies.

in loads estimation. It must be noted that the effect of centrifugal stiffening is important to achieve concordant results, and should therefore not be neglected. The EBBT and GEBT models lead to similar results, with the EBBT predicting slightly less deformations. This is inherent to this beam theory as the initial assumption of neglecting the transverse shear strain typically leads to an underestimation of the deflection. The EBBT will be used in the next sections as it leads to results nearly identical to GEBT for the NREL-5MW turbine at a fraction of the computational cost.

3.2. Impact of the flexibility on the rotor performances in an ABL

In this section, the case of the NREL-5MW wind turbine in a realistic atmospheric boundary layer (ABL) is considered. This case consists of two co-current simulations, as described is Section 2.1. The size of the computational domain is $10D$ in the streamwise direction, $8D$ in the vertical direction and $4D$ in the transverse direction. The main domain grid contains a total of $1024 \times 256 \times 256$ points, and is stretched in the vertical direction above the wind turbine until reaching $\Delta y/D = 0.093$. The ABL has a mean velocity of 9 m/s and a turbulence intensity of 6% at hub height. The turbine rotates at a constant speed of 10.29 rpm. There are 360 time-steps per rotor rotation and the simulation is run for 110 rotations, corresponding to $\simeq$ 640 s. In the following, the EEBT model is used to compare a rigid to a flexible rotor in realistic wind conditions.

The temporal evolution of the blade tip deflections is depicted in Figure 5. The time-averaged

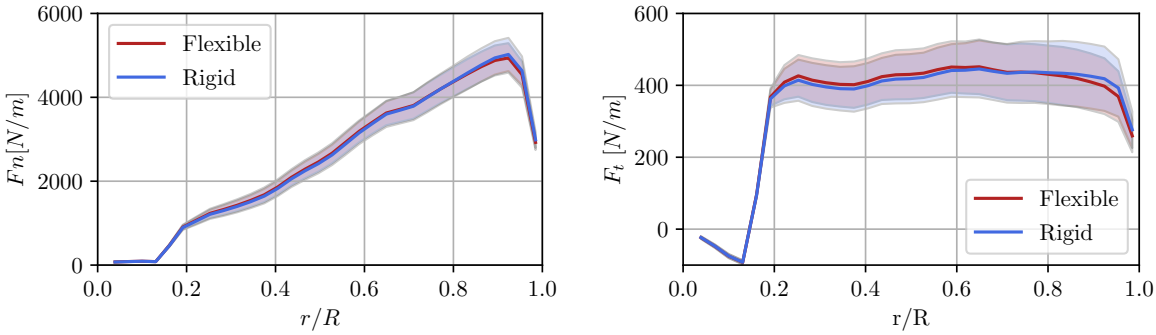


Figure 7: Time-averaged load distribution (solid line) on the turbine blade in the flapwise (left) and edgewise (right) directions. The envelope around the solid line shows the standard deviation.

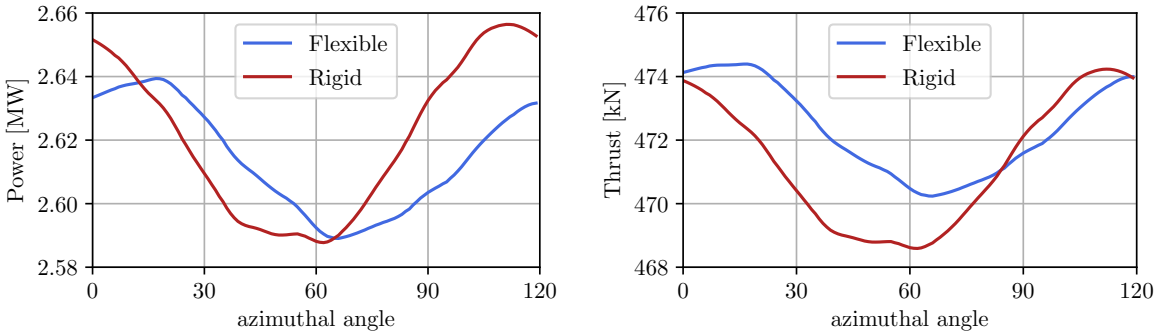


Figure 8: Power and thrust over one third of a rotation, as time-averaged over ~ 50 rotation cycles. The azimuthal angle refers to the angle of one of the three blades

deflection is 3.47 m in the flapwise direction and -0.40 m in the edgewise direction. Most of the variation arises from the rotation of the blade that induces cyclic aerodynamic loads due to the wind shear. Additional variations at different timescales emerging from the turbulent fluctuations of the atmospheric wind can also be observed. Furthermore, it appears that the edgewise deflection presents more oscillations at higher frequencies than the flapwise one.

The power spectral densities (PSD) shown in Figure 6 confirm that the variation of the deformation mostly occurs at the rotation frequency and its first subharmonics. It can also be observed that the first blade eigenfrequency in the flapwise direction coincides with the fourth rotation subharmonic; yet the PSD does not exhibit an increase of the deformation variation at this frequency. On the contrary, in the edgewise direction, the PSD peaks at this first eigenfrequency.

Moreover, a modal decomposition of the blade deflection is carried to analyze the presence of each eigenmode. In the flapwise direction, only the first mode is present, the second mode having a relative weight lower than 0.5%. For the edgewise direction, the weight of the second mode is 3.5%. While this is larger than in the flapwise direction, it remains negligible compared to the first mode. Therefore, it can be stated that the higher bending modes do not significantly participate to the blade deformation, in spite of the turbulent wind fluctuations.

Figure 7 depicts the time-averaged load distribution on the blade for the rigid and the flexible cases. The flexibility induces a small decrease of the loads and their standard deviation at the blade tip. This is explained by the fact that the deflection decreases the angle of attack due to a modification of the blade orientation. On the contrary, the loads are increased on the first part

Table 2: Main results for a row of two turbines: time-averaged and standard deviation of the power, thrust, rotation speed, flapwise and edgewise tip deflections.

	Power [MW]	Thrust [kN]	Rot. speed [rpm]	Flap. u_{tip} [m]	Edge. u_{tip} [m]
WT 1 (flexible)	2.27 (9.4%)	419.3 (6.0%)	9.77 (2.7%)	3.14 (2.2%)	-0.37 (-0.5%)
WT 2 (flexible)	1.09 (18.3%)	265.5 (9.6%)	8.28 (2.1%)	2.19 (4.7%)	-0.24 (-1.3%)
WT 1 (rigid)	2.39 (9.7%)	441.2 (6.1%)	9.93 (2.8%)	-	-
WT 2 (rigid)	1.15 (19.8%)	277.1 (10.2%)	8.34 (2.2%)	-	-

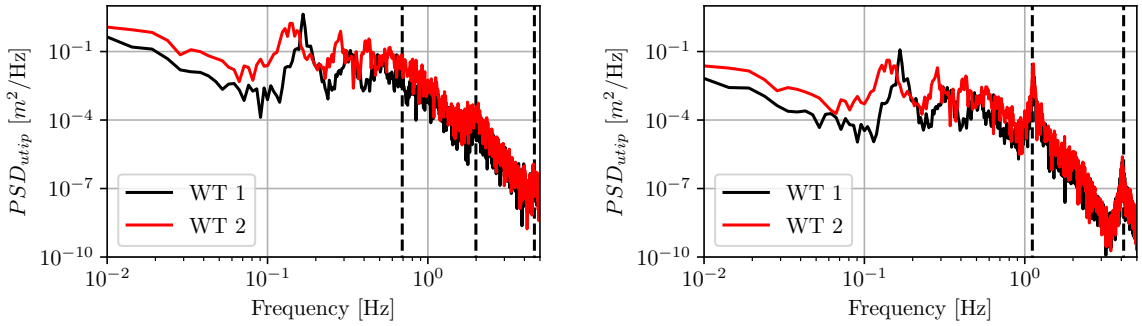


Figure 9: Power spectral density (PSD) of the blade tip deflection in the flapwise (left) and edgewise (right) directions.

of the blade, between $r/R = 0.2$ and 0.6, especially in the edgewise direction. A similar increase was observed in [6, 4, 5], yet it cannot be linked to the minor blade deflection in this region. A possible explanation is the modification of the near wake. The blade tip vortices are moved downstream as a consequence of the flapwise deflection. The inner part of the blade therefore experiences less induced velocity. This highlights the importance of using a flexible actuator curve method to capture the correct aerodynamics of the deformed blade and its near wake.

The time-averaged power and thrust are depicted in Figure 8. The mean value of those quantities is virtually not affect by the flexibility (only a 0.2% difference). The variation within a cycle is however significantly smaller in the case of a flexible rotor: $(P_{max} - P_{min}/P_{mean})$ goes from 2.7% for rigid blades to 1.9% for flexible ones. The thrust varies similarly, but with a smaller amplitude than the power: $(T_{max} - T_{min})/T_{mean}$ is 1.2% for the rigid case, compared to 0.9% for the flexible case. Furthermore, a significant phase shift in the power and thrust are also observed over a revolution cycle. The mean value of the power shift, as computed using the maximum of the cross-correlation between the two signals, is found to be $\simeq 10^o$.

3.3. Two turbines in a row and with wake overlap

In this section, the impact of the flexibility over two turbines in a row is considered. The second turbine intercepts the wake of the preceeding one, and is therefore submitted to larger turbulent fluctuations. The computational set-up for this case is similar to the one described in Section 3.2, except that the size of the domain containing the wind turbines is doubled to accommodate the second one placed $7D$ downstream. A controller is also used that adapt the rotation speed to the wind velocity [14]. The time-step is set to $\Delta t = 0.015$ s and the simulation is run for 720 s.

The time-averaged power, thrust, rotation speed and deflections are reported in Table 2.

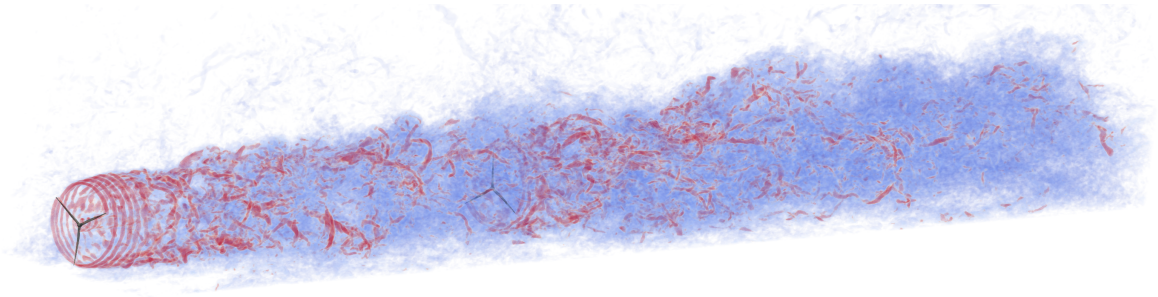


Figure 10: Volume rendering of the vorticity magnitude in the wake of the two rotors.

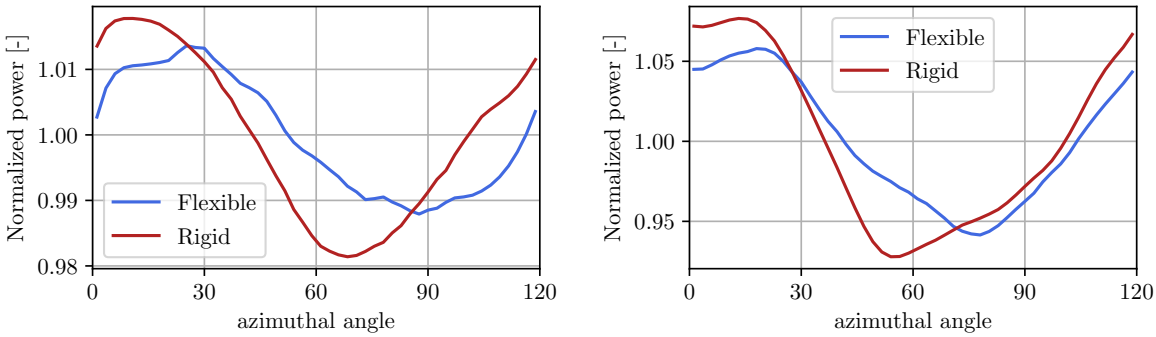


Figure 11: Power (normalized by its mean) of the first (left) and second (right) wind turbines, as time-averaged over ~ 35 rotation cycles.

First, the flexibility tends to reduce the rotation speed, which in turns decreases the mean power and thrust. It can also be observed that the second wind turbine sees its power dropping by $\simeq 52\%$ regardless of flexibility, whereas the standard deviation is almost doubled due to the higher levels of turbulent fluctuations. However, the flexibility mitigates the increase in standard deviation.

A comparison of the power spectral densities of the deflections is depicted in Figure 9. The peaks that correspond to the variation of the deflection during one rotation are shifted towards lower frequencies for the second wind turbine due to the decrease in rotation speed. At higher frequencies, the amplitude of the PSD is larger for the second wind turbine, as a result of the turbulent fluctuations. In the edgewise direction, the peak occurring at the blade eigenfrequency is also more important for the second wind turbine, signaling an increased interaction with the turbulent fluctuations.

Figure 10 shows the magnitude of the vorticity in the wakes of the turbines. The tip vortices of the first wind turbine are well defined due the use of the improved actuator line method. The wake is then destabilized by the wind fluctuations and it becomes fully turbulent. When the flexible actuator curve is used, the position at which the tip vortices are shed is moved downstream due to the flapwise deflection. However, this does not impact the far wake and no differences in mean velocity deficit and turbulent kinetic energy are found behind the rotor.

Finally, Figure 11 displays the averaged power. More variation is observed during a cycle for the second wind turbine, but the flexibility again decreases the amplitude of this variation. The phase shift on the power is still visible for the second wind turbine, but it is decreased compared to that for the first one.

4. Conclusion

We presented an improved and flexible actuator curve model implemented in a LES code, and its application to aeroelastic simulations of the NREL-5MW wind turbine. The actuator curve method is an extension of the actuator line method to curves, and that still uses the 2D Gaussian force distribution to reduce the mollification error. To compute the structural deformations, it is here coupled to a one-dimensional finite element beam model, based either on the Euler-Bernoulli theory or on the geometrically exact theory. After a verification step, the method was used to investigate the effect of flexibility on the NREL-5MW blades in a turbulent atmospheric boundary layer. The flexibility tends to reduce the loads at the blade tip due to the deformation, and a significant phase shift is observed in the power and thrust with regard to the blades azimuthal position. Two turbines in a row were then simulated, and the flexibility is seen to reduce the loads variation on the second wind turbine. A higher interaction with the blade natural frequencies is also noticed due to the increased level of turbulence. A general conclusion is that the flexibility clearly impacts the blade load distribution and the power variation. It has a minimal impact on the far wake. Whereas the aeroelastic effects remain moderate for the considered NREL-5MW turbine, recent larger machines (such as the IEA-15MW turbine model with 120 m blades), thus with a hub also higher (hence more variation of the wind speed between the bottom and the top of the turbine) will exhibit more significant differences. Future work will therefore focus on the application of the developed methodology to those much larger rotors.

Acknowledgments

This research benefited from computational resources made available on the Tier-1 supercomputer of the Fédéeration Wallonie- Bruxelles, infrastructure funded by the Walloon Region under the grant agreement No. 1117545. Computational resources were also provided by the Consortium des Equipements de Calcul Intensif (CECI), funded by the Fonds de la Recherche Scientifique de Belgique under Grant No. 2.5020.11 and by the Walloon Region.

References

[1] Bazilevs Y, Hsu M C, Kiendl J, Wüchner R and Bletzinger K U 2011 *International Journal for numerical methods in fluids* **65** 236–253
[2] Corson D, Griffith D T, Ashwill T and Shakib F 2012 *53rd AIAA/ASME/ASCE/AHS/ASC Structures, Structural Dynamics and Materials Conference 20th AIAA/ASME/AHS Adaptive Structures Conference 14th AIAA* 1827
[3] Heinz J C, Sørensen N N and Zahle F 2013 *PhD thesis, Technical University of Denmark*
[4] Imiela M and Wienke F 2015 Towards multidisciplinary wind turbine design using high-fidelity methods *33rd Wind Energy Symposium* (American Institute of Aeronautics and Astronautics)
[5] Sayed M, Lutz T, Krämer E, Shayegan S, Ghantasala A, Wüchner R and Bletzinger K U 2016 *Journal of Physics: Conference Series* **753** 042009
[6] Dose B, Rahimi H, Herráez I, Stoevesandt B and Peinke J 2018 *Renewable Energy* **129** 591–605 ISSN 0960-1481
[7] Santo G, Peeters M, Van Paepegem W and Degroote J 2019 *Renewable energy* **140** 212–226
[8] Churchfield M J, Lee S, Michalakes J and Moriarty P J 2012 *Journal of turbulence* N14
[9] Storey R, Norris S, Stol K and Cater J 2013 *Wind Energy* **16** 845–864
[10] Vitsas A and Meyers J 2016 *Journal of Physics: Conference Series* **753** 082020 ISSN 1742-6596
[11] Sessarego M, Ramos-García N, Sørensen J N and Shen W Z 2017 *Wind Energy* ISSN 1095-4244
[12] Meng H, Lien F S and Li L 2018 *Renewable energy* **116** 423–437
[13] Spyropoulos N, Papadakis G, Prospathopoulos J M and Riziotis V A 2021 *Applied Sciences* **11** ISSN 2076-3417
[14] Jonkman J, Butterfield S and Musial W 2009 *National Renewable Energy Lab.(NREL)*
[15] Duponcheel M, Bricteux L, Manconi M, Winckelmans G and Bartosiewicz Y 2014 *International Journal of Heat and Mass Transfer* **75** 470 – 482
[16] Moens M, Duponcheel M, Winckelmans G and Chatelain P 2018 *Wind Energy* **21** 766–782
[17] Smagorinsky J 1963 *Monthly Weather Review* **91** 99–164

[18] Sorensen J and Shen W 2002 *ASME. J. Fluids Eng.* 393—399
[19] Jha P K and Schmitz S 2018 *Journal of Fluid Mechanics*
[20] Caprace D G, Chatelain P and Winckelmans G 2019 *AIAA Journal* **57** 17–28
[21] Hodges D H 2006 *Nonlinear Composite Beam Theory* (American Institute of Aeronautics and Astronautics)
[22] Neto M A, Amaro A, Roseiro L, Cirne J and Leal R 2015 *Engineering computation of structures: the finite element method* (Springer)
[23] Balay S, Abhyankar S, Adams M F, Brown J, Brune P, Buschelman K, Dalcin L, Dener A, Eijkhout V, Gropp W D, Kaushik D, Knepley M G, May D A, McInnes L C, Mills R T, Munson T, Rupp K, Sanan P, Smith B F, Zampini S, Zhang H and Zhang H 2021 PETSc users manual Tech. Rep. ANL-95/11 - Revision 3.15 Argonne National Laboratory
[24] Wang Q and Yu W 2017 *Journal of Renewable and Sustainable Energy* **9** 033306
[25] Wang Q, Sprague M A, Jonkman J, Johnson N and Jonkman B 2017 *Wind Energy* **20** 1439–1462
[26] Degroote J 2013 *Archives of computational methods in engineering* **20** 185–238